Cold Regions Science and Technology 178 (2020) 103128

Contents lists available at ScienceDirect

Cold Regions Science and Technology

journal homepage: www.elsevier.com/locate/coldregions

Comparing satellite and helicopter-based methods for observing crevasses, application in East Antarctica

S.S. Thompson[a,*], S. Cook[a], B. Kulessa[b,c], J.P. Winberry[d], A.D. Fraser[a], B.K. Galton-Fenzi[a,e]

[a] Institute for Marine and Antarctic Studies, University of Tasmania, Hobart, Tasmania 7001, Australia
[b] Glaciology Group, College of Science, Swansea University, Singleton Park, Swansea SA2 8PP, UK
[c] School of Technology, Environments and Design, University of Tasmania, Hobart, TAS, 7001, Australia
[d] Department of Geological Sciences, Central Washington University, Ellensburg, WA 98926, USA
[e] Australian Antarctic Division, Kingston, Tasmania 7050, Australia

ARTICLE INFO

Keywords:
Ground-penetrating radar
Synthetic Aperture Radar (SAR)
Crevasses
Field safety

ABSTRACT

Knowing where crevasses are is critical for planning safe on-ice field operations. Previous methods have ranged from real-time imaging of subsurface structures using ground penetrating radar, to mapping of crevasses over large areas using satellite imagery, with each method having it's own strengths and weaknesses. In this paper we compare the detection of crevasses at the Totten Glacier, East Antarctica, from helicopter-borne ground penetrating radar with satellite-based microwave synthetic aperture radar imagery. Our results show that the 80 MHz helicopter-borne ground penetrating radar was able to detect crevasses up to a depth of 70 m, with snow bridge thickness of > 30 m. Comparison with TerraSAR-X (X-band, 9.6 GHz) satellite imagery indicates that the latter is highly effective, detecting 100% of crevasses with snow bridges of up to 4m thick and detecting 95% of crevasses with snow bridges up to 10 m thick. The ability of both methods to identify individual crevasses is affected by several factors including crevasse geometry, survey or satellite orientation and snow moisture content, and further experiments are planned to investigate performance under a wider range of conditions.

1. Introduction

Crevasses are the most conspicuous morphologic feature related to a glacier's dynamic behaviour (Colgan et al., 2016). Crevasses form when the fracture toughness of ice is exceeded (van der Veen, 1998) and thus, their orientation and spacing can be used to study a glaciers stress field (e.g. Vornberger and Whillans, 1990). From an operational and logistics viewpoint, crevasses pose a safety hazard that must be mitigated. Conducting safe field operations in the presence of crevasses is an ongoing challenge for fieldwork in Antarctica and other glaciated regions. Large crevasses may be visible at the surface and therefore be identified remotely. However, snow bridges formed by the accumulation or redistribution of snow make some crevasses challenging to detect from visual inspection. The need for early detection to allow field parties to travel safely has led to the testing and implementation of a wide range of techniques to identify buried crevasses.

Ground-penetrating radar (GPR) has been used to detect crevasses below the surface since the 1970s (Kovacs and Abele, 1974). GPR is particularly effective for identifying subsurface crevasses, as beam spreading causes the radar signal to reflect from the highly reflective crevasse walls rather than relying on the dielectric contrast between air and snow which typically produce weak reflections (Delaney et al., 2004). Many studies report the successful use of GPR for crevasse detection, in both scientific and field safety applications (e.g. Eder et al., 2008; Urbini and Baskaradas, 2010a), and ground-based GPR has a legacy for route-finding applications in Antarctica and Greenland (e.g. Lever et al., 2013; Taurisano et al., 2006; Zamora et al., 2007).

In Antarctica, GPR has typically been used to detect crevasse related hazards in real time, with the radar antenna mounted on the front of a lead traverse vehicle (Delaney et al., 2004; Taurisano et al., 2006; Zamora et al., 2007). The approach requires an operator to continuously monitor the GPR output, and provides only a 2–3 s window for the operator to instruct the driver to stop (Lever et al., 2013). To overcome the issues of operator fatigue and short response time, autonomous robotic vehicles have more recently been developed to independently carry a GPR unit ahead of the field party (Lever et al., 2013; Trautmann et al., 2009). The advantages of such roving vehicles include, further advanced warning of crevassed areas, the ability to systematically survey areas of uncertainty, alternative route finding, and most recently they have also been programmed with machine

* Corresponding author.
E-mail address: ss.thompson@utas.edu.au (S.S. Thompson).

https://doi.org/10.1016/j.coldregions.2020.103128
Received 9 December 2019; Received in revised form 1 June 2020; Accepted 26 June 2020
Available online 01 July 2020

learning to automatically identify crevasses, working toward removing the need for direct operator monitoring (Williams et al., 2012, 2014). However, they currently have limited speed and endurance so can survey only small areas of the ice sheet. Airborne GPR with an antenna mounted to an airplane or helicopter can overcome some of these problems by allowing rapid survey of larger areas (e.g. Urbini et al., 2001).

Helicopter-borne GPR has commonly been used to map seasonal snow cover in glacial (Gusmeroli et al., 2014; Machguth et al., 2006) and non-glacial environments (Lalumiere et al., 1994). In alpine glacial environments helicopter-borne GPR has been used successfully to map the bed at the base of the glacier, necessitating large, low frequency antennas slung beneath the helicopter (Merz et al., 2015a, 2015b; Urbini et al., 2017). While application of helicopter-borne GPR to crevasse detection has been limited, notable exceptions include the International Trans Antarctic Scientific Exploration traverse (Urbini and Baskaradas, 2010a) and the traverse route from McMurdo to South Pole (Delaney and Arcone, 1995).

Another frequently used approach to crevasse detection is the use of satellite imagery, with the potential to rapidly assess a much larger area. Options include visible imagery and photoclinometry which relies on subtle slope changes or shadows to detect the surface expression of crevasses (Bindschadler and Vornberger, 2005) and radar imagery, which penetrates snow and firn (compacted snow) to some extent. Most applications of crevasse detection using satellite imagery have focussed on crevasses which have a visible surface expression. This approach can limit crevasse identification to those features which are open at the surface (e.g. Bhardwaj et al., 2016; Xu et al., 2011). A crevasse with a covering snow bridge can be observed at the surface if the crevasse is sufficiently wide or the snow sufficiently thin that surface slumping occurs. The surface feature can either be detected as a dip in the surface elevation (e.g. Florinsky and Bliakharskii, 2019; Liu et al., 2014) or occasionally as shadows caused by the depression (Merry and Whillans, 1993). However, the method can only observe a snow-bridged crevasse when the width of the crevasse is large relative to the thickness of the snow bridge, thus allowing the bridge to sag and create a visible feature.

A complementary method, requiring less operator training than GPR, is to use radar satellite data collected at microwave wavelengths, which can penetrate below the snow surface. Snow-bridged crevasses have a strong backscatter coefficient in the Ku-band (12–18 GHz), which has been used previously to identify crevasses in Envisat microwave altimeter data (Lacroix et al., 2007). In some examples, the penetration of Envisat's S-band (2–4 GHz) altimeter into the snowpack also allowed a reflection from the base of the snow bridge to be detected. The multiple reflection can allow the thickness of the snow bridge to be calculated, in a similar way to GPR methods (Lacroix et al., 2007).

The Envisat satellite has now been replaced by the Sentinel-1 satellite, operating a microwave synthetic aperture radar. Synthetic aperture radar (SAR) systems emit microwaves on a slant range toward the Earth's surface and measure the backscatter, complete with phase information. The preservation of phase allows synthesis of a higher resolution beam, enabling a ground resolution on the order of 10 m (frequency- and implementation-dependent). The backscatter is highly sensitive to snow properties within the penetration depth of the microwaves. In areas of dry snow, X-band microwaves have been observed to penetrate up to 10 m of snow/firn (Rott et al., 1993). Thus, changes in backscatter caused by crevasses can be detected within the upper 10 m. Satellite-based SAR data has been used in multiple studies to identify crevassing (e.g. Farsund, 2015; Josberger et al., 1994; Koike et al., 2012) and results show buried crevasses can be identified rapidly, over large (10s of km^2) areas, and operate at all times of year and weather conditions. However, the reliability of crevasse detection can depend on the orientation of the crevasse relative to the look direction of the satellite, penetration depth is significantly reduced with increasing snowpack wetness and its ability to resolve individual crevasses depends on the resolution of the satellite data. For example, 25 m resolution RADARSAT radar satellite imagery was found to be less effective than 15 m resolution ASTER optical satellite imagery at identifying crevasses on the South Pole Traverse route (Bindschadler and Vornberger, 2005). Airborne SAR instruments allow even higher spatial resolution backscatter images, enhancing the ability to resolve smaller crevasses (Rohwer et al., 2013; Sander and Bickel, 2007).

In this paper we use data collected by a helicopter-borne GPR system in austral summer 2018/19 to detect subsurface crevasses at the Totten Glacier, East Antarctica, and compare results with X-band SAR satellite data, specifically TerraSAR-X (TSX), to evaluate the effectiveness of the satellite for detecting buried crevasses.

2. Methods

2.1. Field sites

Field sites were chosen based on both accessibility and range of expected crevassing conditions. The Totten Glacier is a large outlet glacier located at (67°30′0.0″ S, 114°0′0.0″ E) which has regions of obvious crevassing open at the surface, as well as large areas where no crevasses are observable in SAR or optical satellite imagery (Fig. 1). Two survey locations were targeted: a) an ice rumple on the floating section of Totten Glacier, where surface conditions transition from apparently crevasse-free ice to open crevasses at the surface, becoming progressively filled by snow as they advect downstream; and b) a region of active subglacial lakes (Wright and Siegert, 2012), where changing topography caused by draining and refilling of the lakes is associated with significant crevassing (Fig. 1).

2.2. GPR

We used an off-the-shelf Måla Ground Explorer GPR system with a shielded high dynamic range (HDR) antenna with a centre frequency of 80 MHz and an inbuilt GPS receiver. The antenna was housed in a wooden box, slung on a 15 m longline from the helicopter cargo hook, the wooden box was flown 15 m from the ground surface, with little surface topography in the region of the surveys we estimate height variation to be ~5 m (Fig. 2). Surveys were carried out in time trigger mode, with a sampling interval of 0.01 s and a ground speed of 75 ± 10 kph, the variability caused by variations in wind speed and direction, resulting in a maximum ground-trace spacing of 0.2 ± 0.03 m.

All GPR data were processed using ReflexW version 8.5 (Sandmeier Scientific Software). Raw data were pre-processed in order to remove repeated traces, pick and reset the glacier surface to time zero and, where applicable, separate into individual profiles for processing. Only basic processing was required to highlight the main features of interest in the GPR data. The processing steps consisted of background removal, to remove the systematic noise introduced by the helicopter (Fig. 3), and dewow, to suppress low-frequency noise. The dewow filter acts on each trace independently; a running mean of a specified window length is calculated for each value of each trace, and then subtracted from it. Here we used a time window of 12 ns. Migration did not improve the data quality and was not applied. Topographic correction was not carried out in this instance as there is little surface slope in the region of the data collection.

The vertical resolution of the GPR system is estimated to be around a half to one-third of the wavelength of the antenna frequency (Annan, 1999). We have no ground-based information regarding radar wave velocity on the Totten glacier. Time-to-depth conversion was performed using an unconstrained average velocity of 200 m μs^{-1}, yielding an average depth penetration of ~70 m. In this region, the snowpack experiences almost no melt (Trusel et al., 2012) and modelled firn depth ranges from 70 to 100 m (Ligtenberg et al., 2011). Firn propagation

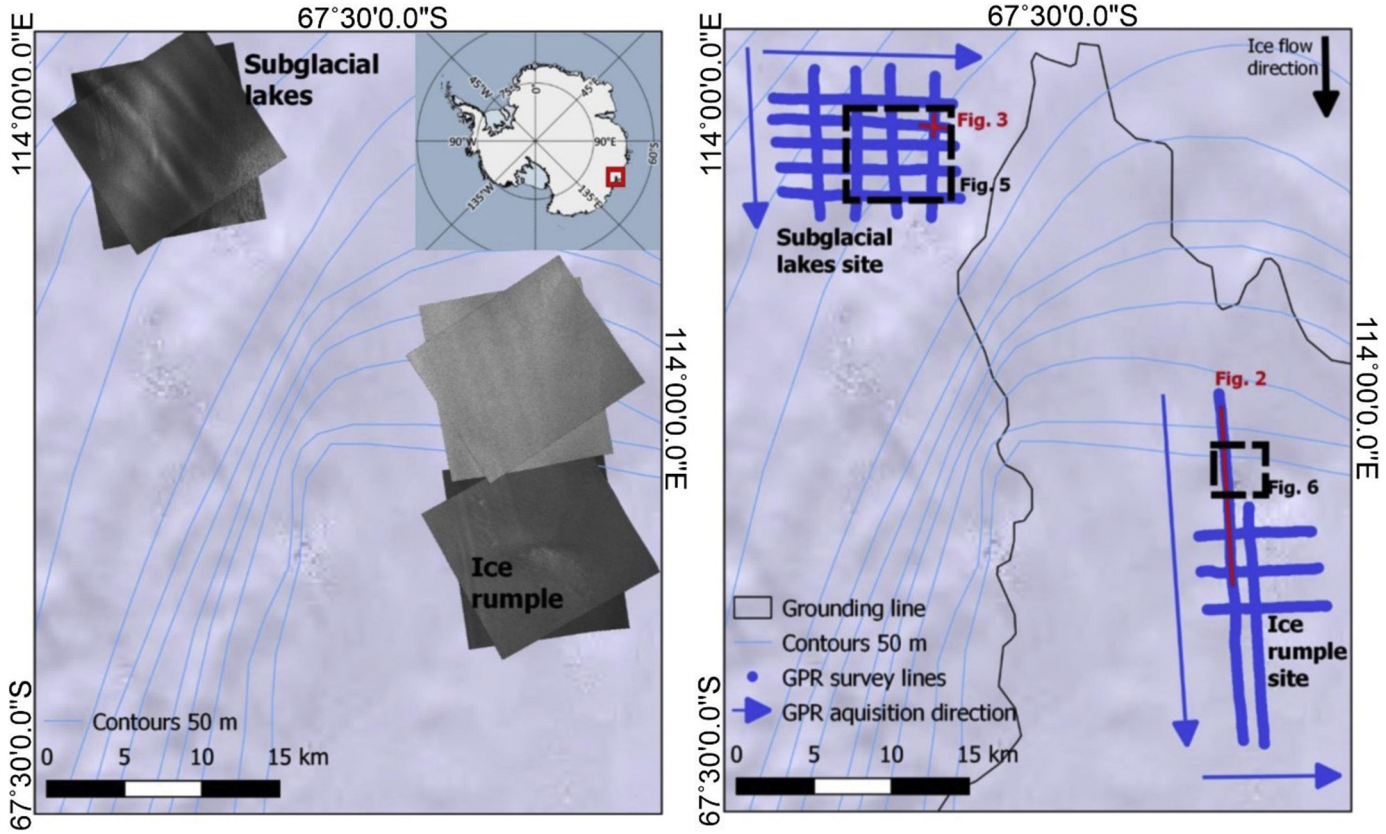

Fig. 1. (a) Totten TSX image locations including both ascending and descending TSX scenes. (b) Totten GPR survey locations, with the locations of the GPR data figures shown in red and the TSX figures in black. Ice flow direction is top to bottom in the figure. Grounding line and contour data is from the SCAR Digital Database and the background is the Landsat LIMA Mosaic. (For interpretation of the references to colour in this figure legend, the reader is referred to the web version of this article.)

velocities can vary widely, strongly dependant on compaction and moisture content (Annan, 1999; Cuffey and Paterson, 2010). Karlsson et al. (2019) measured velocities ranging from 170 to 270 m μs^{-1} using firn cores at Camp Century, Greenland. However, other studies quote values in the region of 190–210 m μs^{-1} (Navarro et al., 2014; Pälli et al., 2003). Using a single wave velocity of 200 m μs^{-1} is likely to be an underestimation at a site with high accumulation and cold conditions with little melt. Using an average of the velocities measured from firn cores at Camp Century (Karlsson et al., 2019), we acknowledge that there could be uncertainty of ~25% in firn velocity and as a result snow bridge thickness may vary by up to 25%. However, the high accumulation, cold conditions at the Totten Glacier suggest more typical firn

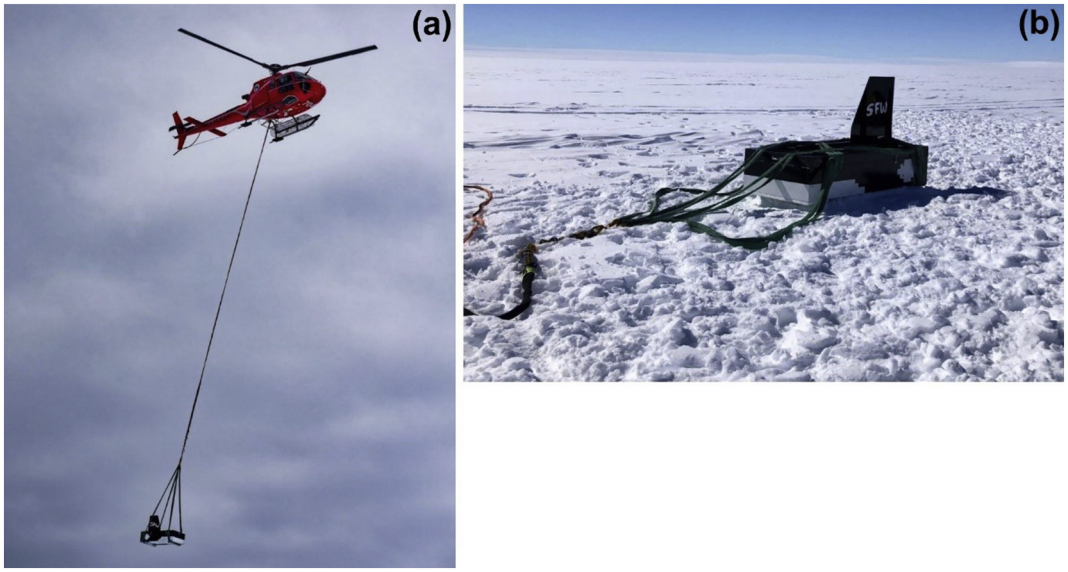

Fig. 2. Helicopter GPR helicopter slinging set up. The 15 m longline was attached to the helicopter cargo hook (a) supported a weighted wooden box housing the antenna (b).

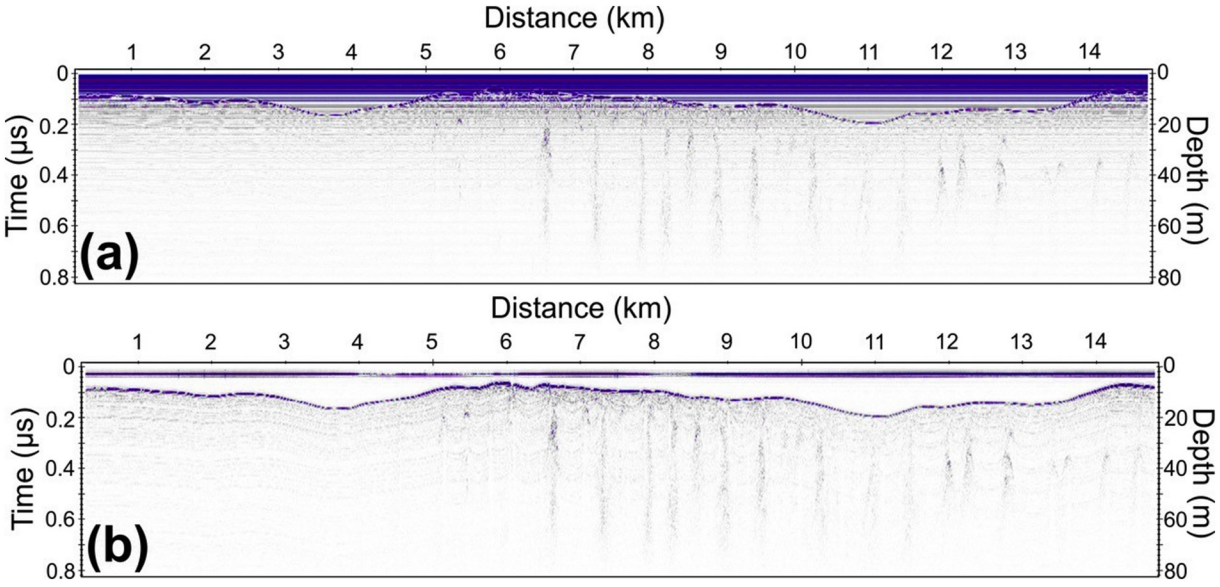

Fig. 3. Systematic noise introduced to the raw data from the helicopter from is removed using the background removal processing step. (a) Raw GPR data from the ice rumple site. (b) Processed GPR data with background removal applied.

Table 1
A list of TSX scenes acquired.

Name	Centre latitude	Centre longitude	Acquisition date	Orbit	Beam	Ascending /descending
ti8_desc	67°34′32.5″ S	113°54′55.1″ E	2018-11-29	87	068R	DESC
ti8_desc	67°34′32.5″ S	113°54′55.1″ E	2019-02-25	82	079R	ASC
ti1d_asc	67°17′06.4″ S	114°14′49.6″ E	2018-12-05	6	070R	ASC
ti1d_desc	67°17′06.4″ S	114°14′49.6″ E	2019-02-26	102	098R	DESC
ti1_desc	67°20′05.6″ S	114°01′10.9″ E	2018-11-29	82	083R	ASC
ti1_asc	67°20′05.6″ S	114°01′10.9″ E	2019-02-25	87	070R	DESC

velocity values in the region of 190–210 m μs^{-1} (Navarro et al., 2014; Pälli et al., 2003), which would result in a velocity and therefore snowbridge thickness uncertainty of ~10%. By under- rather than overestimating we ensure that error in time-to-depth will cause snow bridges to appear thinner and features shallower, a 'safer' approach for on ice operations. Using 200 m μs^{-1} as an estimate of wave velocity in cold, dry firn, provides a wavelength of ~2.5 m in the firn, giving a vertical resolution of ~0.84 to 1.25 m. Horizontal resolution is defined as the diameter D of the first Fresnel zone, as is estimated by Fowler (1990):

$$D = \sqrt{2Z\lambda + \frac{\lambda^2}{4}} \quad (1)$$

where Z is depth and λ is the antenna wavelength, both in metres. At a depth of 10 m the horizontal resolution of our GPR system is ~8 m.

Processing uncertainties can be introduced while picking features and conducting time-to-depth conversion of the GPR data. Picking is subjective, and its quality depends on the sharpness of the reflectors (Gusmeroli et al., 2012; Schannwell et al., 2014). Crevassed areas with multiple reflections make picking upper edges of the crevasses challenging and therefore reduce the precision of depth estimates. Using a constant velocity of 200 m μs^{-1} will introduce errors due to the transition from fresh snow at the surface through to compacted firn at depth. However, we do not have sufficient information to develop a variable radio wave velocity with changing firn compaction at depth. Additional uncertainty in crevasse location can arise from GPS locational accuracy of the antenna, and from the potential change in angle arising from swinging of the antenna under sling-loading conditions (estimated to be ~10 m based on visual observations).

2.3. SAR

SAR data were acquired from the X-band (9.65 GHz) TerraSAR-X satellite (TSX). The Spotlight-mode images used here have a slant range resolution of 1.2 m and an azimuth resolution of 1.7 m. As indicated in Fig. 1, three TSX image footprints cover the two survey sites at the Totten Glacier. For each footprint both ascending and descending data were acquired (Fig. 1; Table 1). Ascending and descending images have a different azimuth angle and are therefore sensitive to crevasses of different alignment. All data were acquired in HH single polarisation mode and provided as Enhanced Ellipsoid Corrected Geotiff files to minimise locational uncertainty due to topography.

SAR images have a natural "speckle" which is caused by the sensitivity of the measurement to small, phase-coherent changes in the backscatter. Speckle can make image interpretation challenging, therefore the TSX images were smoothed to reduce the speckle noise, using guided filtering over blocks of 10 × 10 pixels. Guided filtering is an edge-preserving smoothing method which is designed to remove random noise, while retaining linear features in the image such as crevasses (He et al., 2013). Crevasses were identified in the despeckled TSX imagery via visual inspection and therefore their identification involved an element of subjectivity due to the personal interpretation and identification of the inspector. In all cases, when a crevasse was detected in the GPR data, crevasses were also visible nearby in the TSX data, indicating that even when TSX is unable to identify individual crevasses it is still able to delineate areas where crevasses are likely to be present.

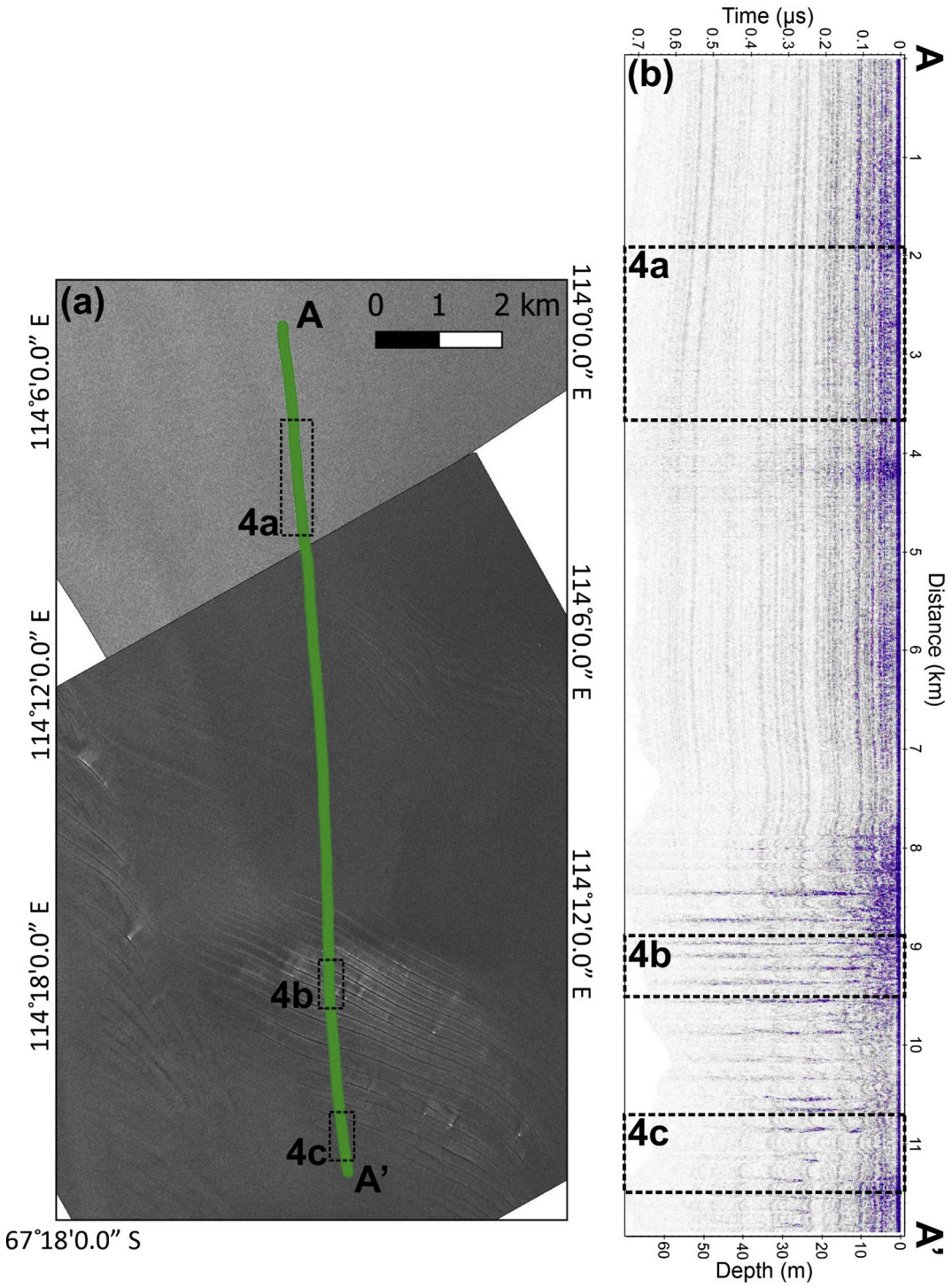

Fig. 4. The location of a line of GPR data, over TSX imagery, transiting from a crevasse-free to a crevassed glacier zone on the floating portion of the Totten Glacier (location shown in red in Fig. 1). Ice flow direction along the full profile A-A′ (right side) is from A to A′. Sections 4a-c refer to the locations of the sections in Fig. 5. (For interpretation of the references to colour in this figure legend, the reader is referred to the web version of this article.)

3. Results

3.1. Crevasse detection from GPR

Both crevasse-free and crevassed zones are visible in the GPR data at the Totten Glacier. In crevasse-free regions the dominant features are horizontally continuous reflections (Figs. 4 & 5a), attributed to layers of different character within the firn. Snow (firn) bridges and crevasses are also apparent, and bridge thickness varies from zero (crevasse is open at the surface) to more than 30 m thick (Fig. 5c). Crevasse features identified in the GPR data are variable in form, and at least three different crevasse morphologies are evident. Immediately upstream of the ice rumple, there is a transition from crevasse-free ice (Fig. 4), to crevasse features of regular, straight-sided morphology, roughly 5 m wide, identified by a break in the horizontal returns (Fig. 4a). These are analogous in shape to the “new cracks” identified by (Delaney et al., 2004), although excavation of these “new cracks” by hot water drill revealed them to measure between 0.1 and 0.5 m across (Delaney et al.,

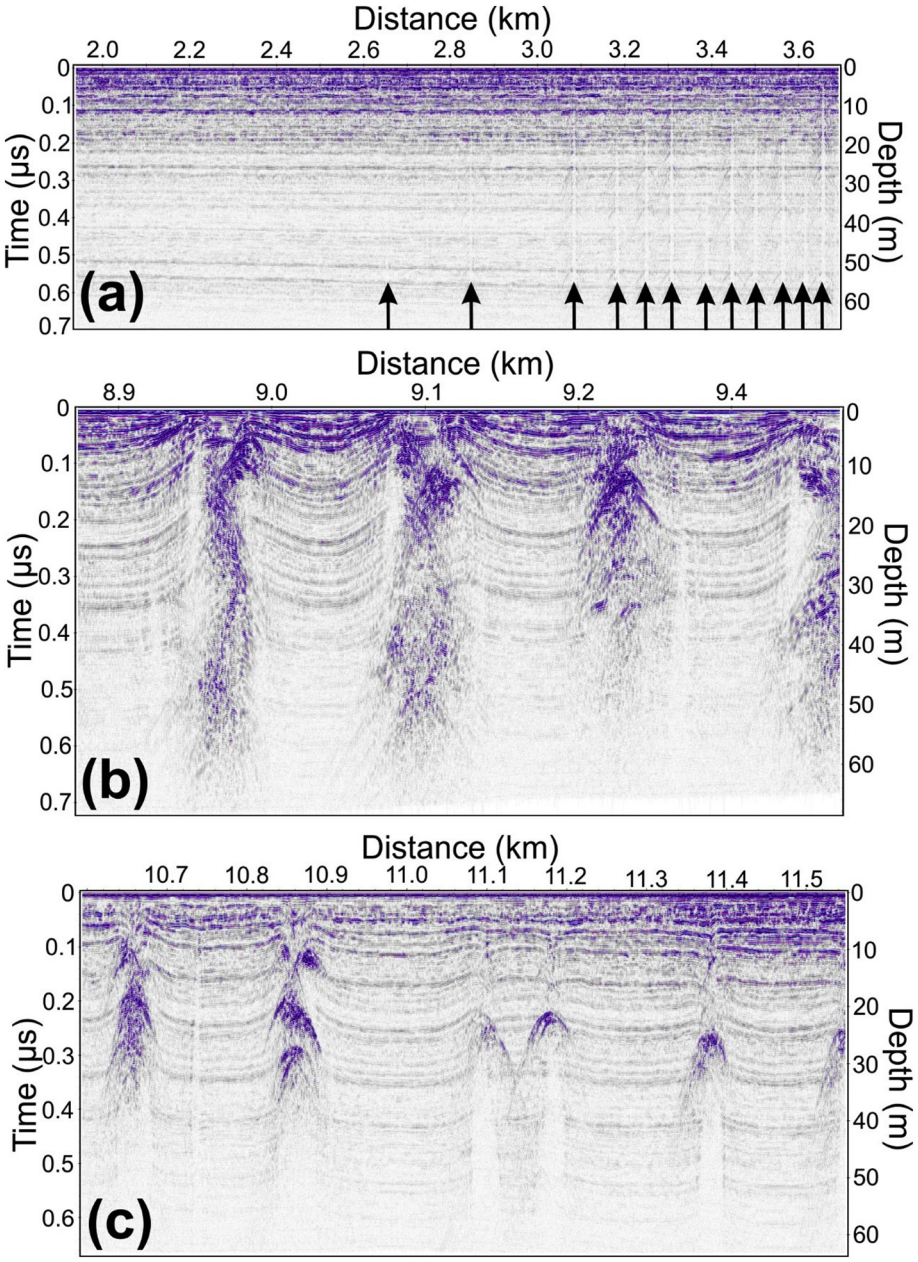

Fig. 5. Section of GPR data located along Fig. 2 profile, illustrating the various crevasse signatures observed in the GPR data. Arrows in (a) highlight the location of the crevasse features of regular, straight-sided morphology.

2004), a magnitude smaller in width then the features identified in Fig. 5a.

Around the ice rumple, where crevasse features are large and shallow enough to be identified in visible wavelength satellite imagery as well as TSX (Fig. 4a), the crevasses appear in the GPR data as large, chaotic energy returns > 50 m wide and the radar signal appears to reflect from multiple surfaces (Fig. 5b). The horizontally continuous reflections in between these features appear to sag, giving a convex appearance to the firn layering (Fig. 5b). Toward the downflow end of the profile (Fig. 4), crevasses with a distinct hyperbola at the crevasse apex and fewer chaotic reflections are visible. The crevasses are found at greater depths beneath the surface with a clear disturbance in the firn layers above the crevasse opening (right side Fig. 5c). In this region, the horizontally continuous reflections between the features still appear to sag at depth but as the snow bridge thickens and the crevasses become increasing buried the horizontally continuous reflections closer to the surface appear flatter (Fig. 5c).

The grid-based survey conducted over the subglacial lakes provided GPR data both perpendicular to and along the line of the dominant crevasse orientation. At this site, the expression of crevasses in the GPR data is very different depending on the orientation of the survey line relative to crevasses (Fig. 6). Where survey lines are roughly perpendicular to crevasse strike, they have the distinctive hyperbola-shaped return in the GPR data (Fig. 6 B-B′). However, their spatial pattern and snow bridge thickness is much more variable than those identified in the region of the ice rumple (Fig. 5). In survey lines orientated roughly parallel to crevasse strike, the presence of crevasses is evident in the GPR data but their form is much more complex than the shape of a hyperbola, and it is difficult to discern individual features (Fig. 6 C-C′).

3.2. Crevasse detection from TSX

Over the two survey areas at the Totten Glacier, 912 crevasses were detected in the GPR profiles, with maximum snow bridge thicknesses

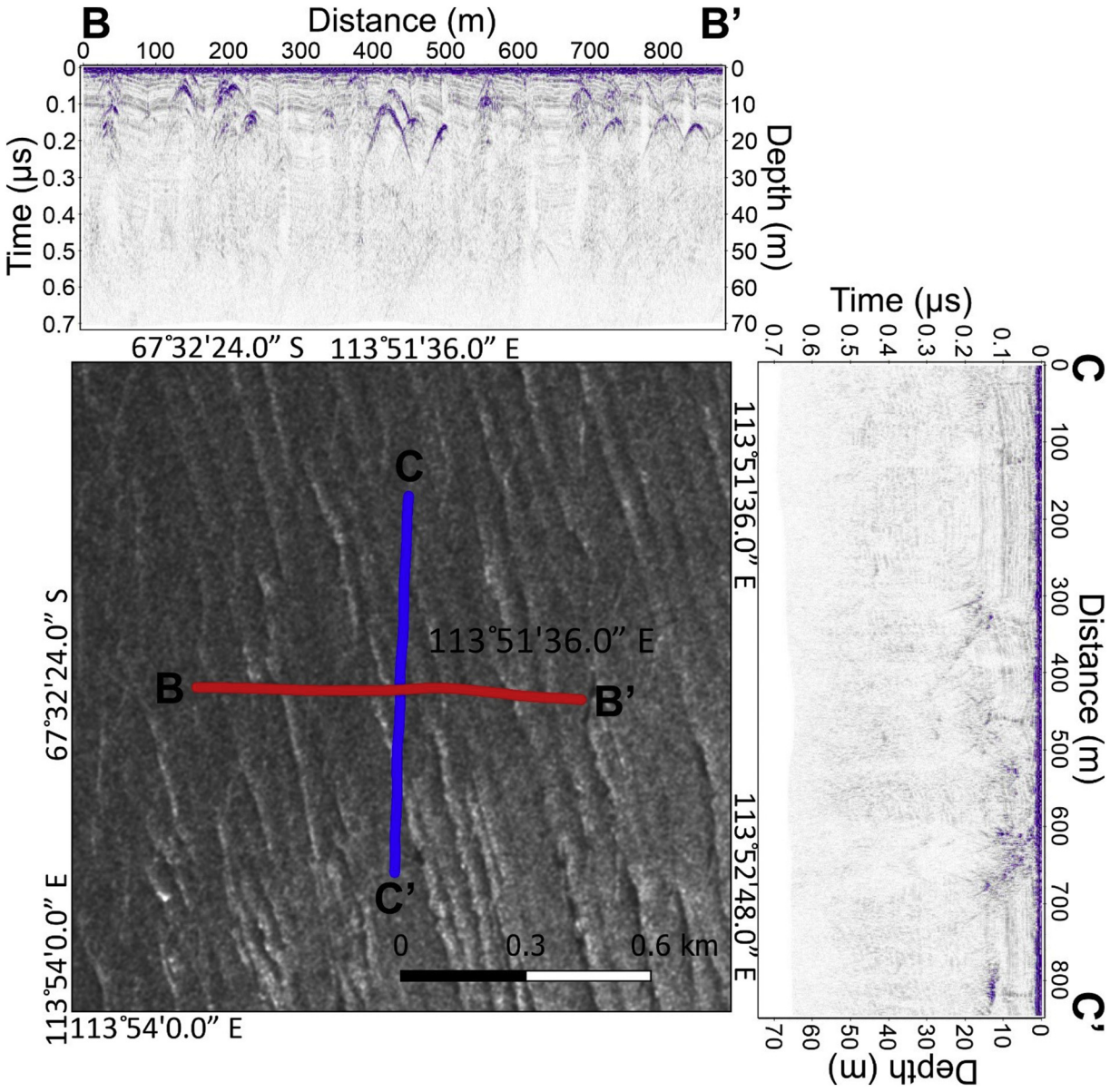

Fig. 6. The location of two GPR profiles from the subglacial lake crevassed site over TSX data, collected along two different orientations. Line B-B′ runs roughly perpendicular to crevasse orientation and line C-C′ in line with crevasse orientation (location shown in red in Fig. 1). (For interpretation of the references to colour in this figure legend, the reader is referred to the web version of this article.)

Table 2
Comparison of crevasses detected in the GPR data with both ascending and descending TSX data. Non-regular grouping of snow bridge thickness reflects the focus on crevasses with thinner snow-bridges for field operations.

Snowbridge thickness (m)	GPR crevasses	Ascending TSX data		Descending TSX data	
		TSX visible	TSX non-visible	TSX visible	TSX non-visible
0–1	25	24	1	25	0
1–2	85	81	4	85	0
2–4	59	58	1	59	0
4–10	183	148	35	173	10
10–20	384	226	156	283	101
20–30	130	42	90	46	84
30+	46	6	40	5	41
Total	912	585	327	676	236
%		64	36	74	26

of > 30 m (Table 2; Fig. 7). All GPR-identified crevasse locations were plotted over the TSX images, of which 585 and 676 were visible in the ascending and descending TSX images respectively (Table 2; Fig. 7). Up to a snow bridge thickness of ~4 m all crevasses were identifiable in the descending TSX data and 96% of them in the ascending data (Table 2; Fig. 7). In the descending data 93.6% of crevasses were detected up to a snow bridge thickness of ~20 m, (ascending data: 85.8%) (Table 2; Fig. 7). It was not possible to determine a relation between crevasse width and visibility in the TSX data, likely due to variability in snow bridge thickness and crevasse morphology.

4. Discussion

At the sites at the Totten Glacier crevasses are clearly identifiable in both the GPR data and the TSX data, and their expression allows an initial classification to be made between crevassed and crevasse-free zones. Crevasses in the GPR data have variable signatures (Fig. 5), associated with different snow and firn properties, crevasse morphology

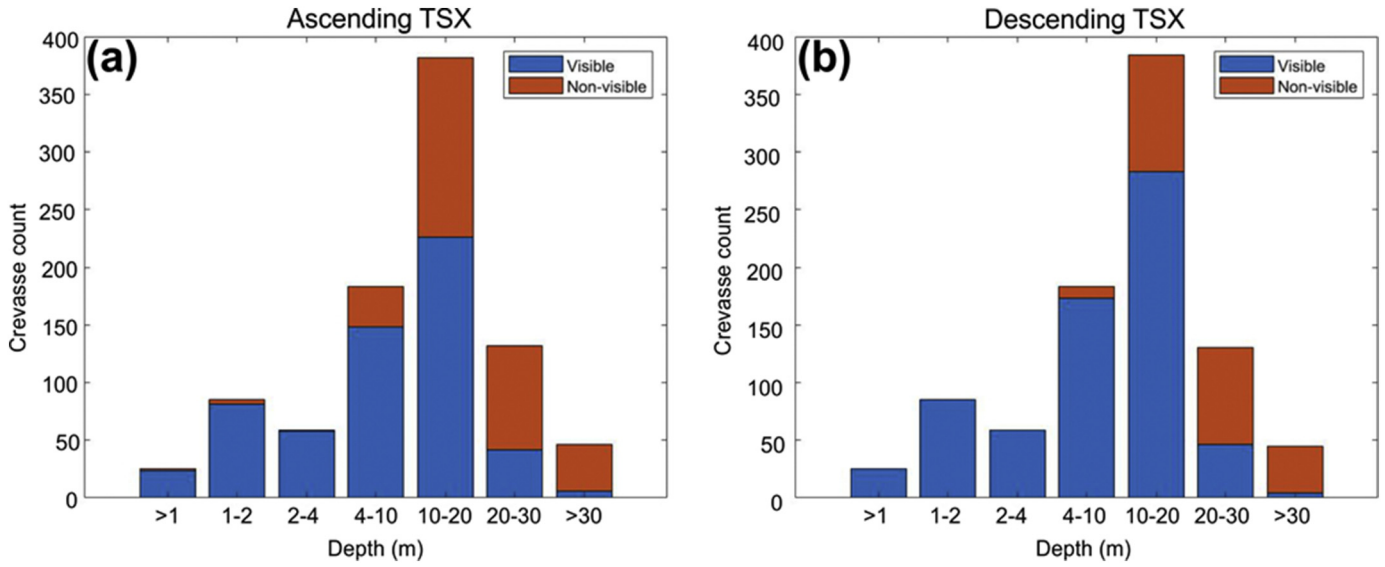

Fig. 7. Number of crevasses detected in GPR surveys, grouped by snow-bridge thickness (depth beneath the surface), indicating proportion visible in TSX ascending and descending data.

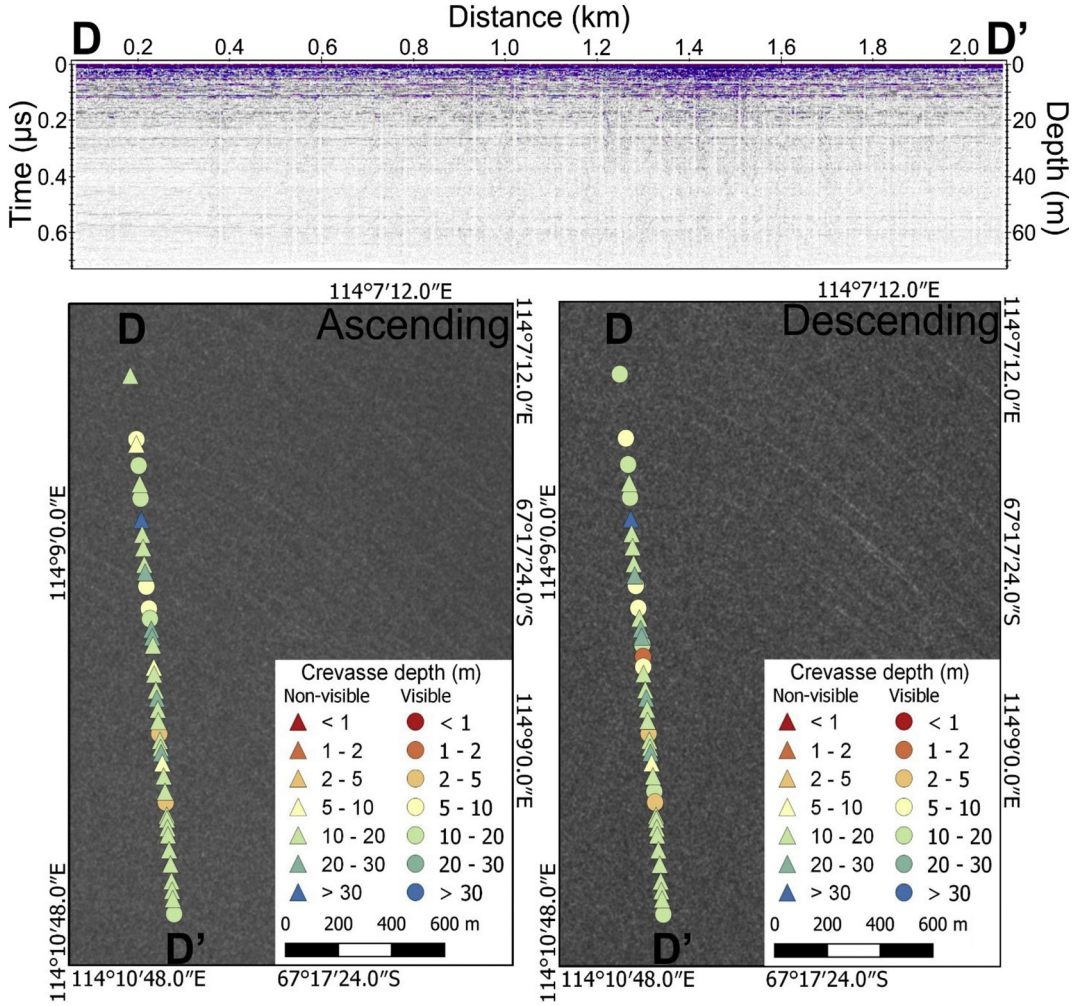

Fig. 8. GPR data along section D-D′ and the corresponding crevasse location and snow bridge thickness for the narrow crevasses identified in the GPR data upglacier from the ice rumple overlain on TSX data.

and orientation to flight path (as previously identified by Delaney et al. (2004)). The survey over the subglacial lakes illustrates that individual crevasses are less distinct when flying along rather than across their strike (Fig. 6 B-B′). While predictions of likely crevasse orientation can be made by examining ice velocity and incorporated into survey design, surveys should be conducted at a minimum of two orthogonal (preferably more) directions. Where knowledge of crevasse geometry and precise location is required, this approach would ensure that all crevasses have been approached in a direction other than normal to their strike. The flexibility of helicopter-borne GPR allows immediate investigation of any ambiguous features in the data and the ability to adjust survey locations and angles where needed.

Automation of crevasse detection in GPR data will be strongly affected by the variability in crevasse morphology. For example, the narrow crevasses located on the right-hand side of Fig. 5a do not have strong reflective parabolas, appearing instead as a vertical gap in the surrounding horizontal firn layers. Identification of these crevasses therefore requires particular care, especially during real time acquisition. An important consideration for automated crevasse detection should therefore be examination for breaks in horizontal firn layers as well as parabolas created by crevasse wall reflections (Williams et al., 2012).

Crevasse detection from the TSX data surpassed the expected range in snow bridge thickness, detecting crevasses below the reported TSX snow penetration limit of 10 m (based on previous work e.g. Rott et al. (1993)). The performance is related firstly to the cold, dry conditions found at the Totten Glacier, optimal for maximising penetration depth. Secondly, visibility is likely enhanced by disturbance in the firn layers of the snow bridge above crevasses, evident in the GPR data (Figs. 4, 5), causing enough backscatter to allow detection of the expression of crevasses below the microwave penetration limit.

Even in areas where not all crevasses detected by the GPR were observed by TSX, the satellite method shows clear potential as a reliable method for field safety applications. Around the ice rumple site, mid-depth crevasses (5–10 m snow bridge) were visible in GPR data but not in TSX. However, crevasses are clearly visible in the TSX images to the side of the survey line (right side of Fig. 8). The angle of the features suggests that they intersect the location of the crevasses identified in GPR data (Fig. 8). One potential use of the TSX images would be to identify an area of uncertainty around visible crevasses, requiring further investigation to determine the extent of the crevassed zone.

Similar to the GPR data, detectability of crevasses in TSX data is also dependant on the relative orientation of the crevasses to the satellite path (Fig. 8; Table 2). Across both sites at the Totten Glacier the descending TSX data performed slightly better than the ascending TSX over a snow bridge thickness of ~4 m, detecting 68% compared to 57% of crevasses visible in the GPR data (Fig. 8; Table 2). The relative performance of ascending and descending images will depend on the crevasse orientation relative to satellite look angle, necessitating the acquisition of both ascending and descending data for all new crevasse detection sites. In addition, the geometry of a crevasse will impact its visibility in SAR data. Brock (2010), using airborne X-band SAR concluded “the crevasse walls can be efficient scattering surfaces, but whether a significant portion of the scattered energy is scattered back to the radar depends on the details of the geometry”. In many cases the base of the snow bridge provided a stronger return than the crevasse walls, dependant on both the geometry of the crevasse walls and the instrument incidence angle.

The cold-dry snow conditions at the Totten Glacier are ideal for the application of TSX and the approach has significant value, however, microwave absorption is strongly affected by the presence of liquid water, and moisture in the snowpack will substantially reduce the penetration depth. The penetration depth will also depend to some extent on the presence of chemical impurities, which can vary significantly between locations (Brock, 2010). The local surface roughness also has an impact on the visibility of subsurface crevasses. As the microwave signal propagates into the snowpack it experiences loss due to absorption and scattering, reducing the intensity of features observed at depth. If the snow surface exhibits significant roughness, then it is possible that subsurface objects will be difficult to distinguish from surface “clutter” (Brock, 2010).

5. Conclusions

Application of helicopter-borne GPR and satellite-based microwave SAR to crevasse detection at the Totten Glacier, East Antarctica confirms that both approaches can be effective for crevasse detection. Crevasses were identifiable in GPR surveys to a depth of ~70 m below the surface, with snow bridges over 30 m thick. Detection of individual crevasses is affected by both the crevasse size and orientation relative to helicopter or satellite flight path. However, helicopter-borne methods have sufficient flexibility in approach angles to thoroughly investigate any crevassing.

TSX data proved highly effective in identifying crevasses with snow bridges of up to ~4 m thick and detected the majority of crevasses with snow bridges up to ~10 m thick. There are significant possibilities of using microwave SAR data for efficient field site planning over much larger areas of the ice sheet where a presence or absence of crevassing is required. The use of SAR satellite imagery is a significant benefit to field planning, covering large areas at a significantly lower cost than ground-based or airborne approaches and is applicable through all seasons and weather conditions. Helicopter-borne GPR can pass a crevassed area at a range of speeds and approach angles to thoroughly investigate crevassing. In addition to the simple presence or absence of crevasses, GPR has the added value of providing more precise information on crevasse extent, width and snow bridge thickness. Many on-ice applications in Antarctica, and elsewhere, require working within crevasse zones or over-ice traversing vital for assessing field safety and route finding in crevassed areas. The combination of both techniques can provide a powerful approach. Analysis of TSX data can quickly and efficiently highlight zones of crevassed vs crevasse-free ice and areas of uncertainty where further investigation is needed to inform decision making and route finding. Helicopter-borne GPR can then be focused in such areas, providing the required level of detail and flexibility, whilst minimising costs and refuelling constraints.

The performance of both techniques depends on crevasse orientation and geometry relative to acquisition angle, and detectability may be significantly hampered in areas with high snow moisture content. Further investigation is needed to quantify the effect of snow moisture content and constrain estimates of crevasse geometry and snow bridge thickness.

Declaration of Competing Interest

The authors declare that they have no known competing financial interests or personal relationships that could have appeared to influence the work reported in this paper.

Acknowledgements

This work was funded by the Australian Research Council's Special Research Initiative for the Antarctic Gateway Partnership (project ID SR140300001). Geophysical data collection was supported through the Australian Government's Australian Antarctic Program under project AAS 5145. TerraSAR-X satellite data were provided by DLR under project HYD3606, thanks to Erhard Diedrich, Paul Wachter and Ursula Marschalk for help in setting this up.

References

Annan, A.P., 1999. Practical processing of GPR data. Proceedings of the Second Government Workshop on Ground Penetrating Radar 1–16.

Bhardwaj, A., Sam, L., Singh, S., Kumar, R., 2016. Automated detection and temporal monitoring of crevasses using remote sensing and their implications for glacier dynamics. Ann. Glaciol. 57, 81–91. https://doi.org/10.3189/2016AoG71A496.
Bindschadler, R., Vornberger, P., 2005. Guiding the south pole traverse with ASTER imagery. J. Glaciol. 51, 179–180.
Brock, B.C., 2010. On the Detection of Crevasses in Glacial Ice with Synthetic-aperture Radar.
Colgan, W., Rajaram, H., Abdalati, W., Mccutchan, C., Mottram, R., Moussavi, M.S., Grigsby, S., 2016. Glacier crevasses: observations, models, and mass balance implications. Rev. Geophys. 54, 119–161. https://doi.org/10.1002/2015RG000504.
Cuffey, K.M., Paterson, W.S.B., 2010. The Physics of Glaciers, 4th ed. Elsevier.
Delaney, A.J., Arcone, S.A., 1995. Detection of crevasses near McMurdo Station, Antarctica with airborne short-pulse radar. In: Sixth Symposium on Antarctic Logistics and Operations, pp. 29–31.
Delaney, A.J., Arcone, S.A., O'Bannon, A., Wright, J., 2004. Crevasse detection with GPR across the Ross Ice Shelf, Antarctica. In: Proc. Tenth Int. Conf. Grounds Penetrating Radar, 2004. GPR 2004, pp. 777–780. https://doi.org/10.1109/ICGPR.2004.179867.
Eder, K., Reidler, C., Mayer, C., Leopold, M., 2008. Crevasse detection in Alpine areas using GPR as a component for a mountain guide system. Int. Arch. Photogramm. Remote Sens. Spat. Inf. Sci. Beijing XXXVII, 1–6.
Farsund, I., 2015. Crevasses on Svalbard Glaciers : Distribution and Dynamic Controls. University of Bergen.
Florinsky, I.V., Bliakharskii, D.P., 2019. Detection of crevasses by geomorphometric treatment of data from unmanned aerial surveys. Remote Sens. Lett. 10, 323–332. https://doi.org/10.1080/2150704X.2018.1552809.
Fowler, C.M.R., 1990. The Solid Earth an Introduction to Geophysics, 1st ed. Cambridge University Press.
Gusmeroli, A., Jansson, P., Pettersson, R., Murray, T., 2012. Twenty years of cold surface layer thinning at Storglaciären, sub-Arctic Sweden, 1989-2009. J. Glaciol. 58, 3–10. https://doi.org/10.3189/2012jog11j018.
Gusmeroli, A., Wolken, G.J., Arendt, A.A., 2014. Helicopter-borne radar imaging of snow cover on and around glaciers in Alaska. Ann. Glaciol. 55, 78–88. https://doi.org/10.3189/2014aog67a029.
He, K., Sun, J., Tang, X., 2013. Guided image filtering. IEEE Trans. Pattern Anal. Mach. Intell. 35, 1397–1409. https://doi.org/10.1109/TPAMI.2012.213.
Josberger, E.G., True, M.A., Shuchman, R.A., 1994. Determination of surface features on glaciers in Alaska from ERS-1 SAR observations. In: Proceedings of IGARSS'94–1994 IEEE International Geoscience and Remote Sensing Symposium. 4. IEEE, pp. 2398–2400. https://doi.org/10.1109/igarss.1994.399749.
Karlsson, N.B., Colgan, W.T., Binder, D., Machguth, H., Abermann, J., Hansen, K., Pedersen, A., 2019. Ice-penetrating radar survey of the subsurface debris field at Camp Century, Greenland. Cold Reg. Sci. Technol. 165, 102788. https://doi.org/10.1016/j.coldregions.2019.102788.
Koike, K., Yoshida, H., Omura, M., Shibuya, K., Doi, K., 2012. Temporal changes in crevasses in the middle Slessor Glacier, Coats Land, East Antarctica through SAR data analysis. Earth Planet. Sp. 64, 257–267. https://doi.org/10.5047/eps.2011.10.003.
Kovacs, A., Abele, G., 1974. Crevasse detection using an impulse radar system. Antarct. J. 177–178 July-Augus.
Lacroix, P., Legrésy, B., Coleman, R., Dechambre, M., Rémy, F., 2007. Dual-frequency altimeter signal from Envisat on the Amery ice-shelf. Remote Sens. Environ. 109, 285–294. https://doi.org/10.1016/j.rse.2007.01.007.
Lalumiere, L., Rossiter, J., Prinsenberg, S., 1994. Airborne snow thickness radar. In: Fifth International Conferention on Ground Penetrating Radar.
Lever, J.H., Delaney, A.J., Ray, L.E., Trautmann, E., Barna, L.A., Burzynski, A.M., 2013. Autonomous GPR surveys using the polar rover Yeti. J. F. Robot. 30, 194–215. https://doi.org/10.1002/rob.
Ligtenberg, S.R.M., Helsen, M.M., Van Den Broeke, M.R., 2011. An improved semi-empirical model for the densification of Antarctic firn. Cryosphere 5, 809–819. https://doi.org/10.5194/tc-5-809-2011.
Liu, Y., Cheng, X., Hui, F., Wang, X., Wang, F., Cheng, C., 2014. Detection of crevasses over polar ice shelves using Satellite Laser Altimeter. Sci. China Earth Sci. 57, 1267–1277. https://doi.org/10.1007/s11430-013-4796-x.
Machguth, H., Eisen, O., Paul, F., Hoelzle, M., 2006. Strong spatial variability of snow accumulation observed with helicopter-borne GPR on two adjacent Alpine glaciers. Geophys. Res. Lett. 33, 1–5. https://doi.org/10.1029/2006GL026576.
Merry, C.J., Whillans, I.M., 1993. Ice-flow features on Ice Stream B, Antarctica, revealed by SPOT HRV imagery. J. Glaciol. 39, 515–527. https://doi.org/10.1017/S0022143000016415.
Merz, K., Green, A.G., Buchli, T., Springman, S.M., Maurer, H., 2015a. A new 3-D thin-skinned rock glacier model based on helicopter GPR results from the Swiss Alps. Geophys. Res. Lett. 42, 4464–4472. https://doi.org/10.1002/2015GL063951.
Merz, K., Maurer, H., Buchli, T., Horstmeyer, H., Green, A.G., Springman, S.M., 2015b. Evaluation of ground-based and helicopter ground-penetrating radar data acquired across an alpine rock glacier. Permafr. Periglac. Process. 26, 13–27. https://doi.org/10.1002/ppp.1836.
Navarro, F.J., Martín-Español, A., Lapazaran, J.J., Grabiec, M., Otero, J., Vasilenko, E.V., Puczko, D., 2014. Ice volume estimates from ground-penetrating radar surveys, Wedel Jarlsberg Land Glaciers, Svalbard. Arctic Antarct. Alp. Res. 46, 394–406. https://doi.org/10.1657/1938-4246-46.2.394.
Pälli, A., Moore, J.C., Rolstad, C., 2003. Firn-ice transition-zone features of four polythermal glaciers in Svalbard seen by ground-penetrating radar. Ann. Glaciol. 37, 298–304. https://doi.org/10.3189/172756403781816059.
Rohwer, J.A., Thompson, M., Bickel, D.L., Bielek, T.P., Sander, G.J., 2013. An X-band crevasse detection radar for the Arctic and Antarctic. IEEE Natl. Radar Conf. - Proc. https://doi.org/10.1109/RADAR.2013.6586035.
Rott, H., Sturm, K., Miller, H., 1993. Active and passive microwave signatures of Antarctic firn by means of field measurements and satellite data. Ann. Glaciol. 17, 337–343.
Sander, G.J., Bickel, D.L., 2007. Antarctica X-band MiniSAR Crevasse Detection Radar : Final Report. pp. 1–42.
Schannwell, C., Murray, T., Kulessa, B., Gusmeroli, A., Saintenoy, A., Jansson, P., 2014. An automatic approach to delineate the cold-temperate transition surface with ground-penetrating radar on polythermal glaciers. Ann. Glaciol. 55, 89–96. https://doi.org/10.3189/2014AoG67A102.
Taurisano, A., Tronstad, S., Brandt, O., Kohler, J., 2006. On the use of ground penetrating radar for detecting and reducing crevasse-hazard in Dronning Maud Land, Antarctica. Cold Reg. Sci. Technol. 45, 166–177. https://doi.org/10.1016/j.coldregions.2006.03.005.
Trautmann, E., Ray, L., Lever, J., 2009. Development of an autonomous robot for ground penetrating radar surveys of polar ice. In: 2009 IEEE/RSJ Int. Conf. Intell. Robot. Syst, pp. 1685–1690. https://doi.org/10.1109/IROS.2009.5354290.
Trusel, L.D., Frey, K.E., Das, S.B., 2012. Antarctic surface melting dynamics: Enhanced perspectives from radar scatterometer data. J. Geophys. Res. Earth Surf. 117, 1–15. https://doi.org/10.1029/2011JF002126.
Urbini, S., Baskaradas, J.A., 2010a. GPR as an effective tool for safety and glacier characterization: Experiences and future development. In: Proc. 13th Internarional Conf. Gr. Penetrating Radar, GPR 2010, pp. 1–6. https://doi.org/10.1109/ICGPR.2010.5550268.
Urbini, S., Vittuari, L., Gandolfi, S., 2001. GPR and GPS data integration: examples of application in Antarctica. Ann. Geophys. 44 (4), 687–702. https://doi.org/10.4401/ag-3568.
Urbini, S., Zirizzotti, A., Baskaradas, J.A., Tabacco, I.E., Cafarella, L., Senese, A., Smiraglia, C., Diolaiuti, G., 2017. Airborne radio echo sounding (RES) measures on alpine glaciers to evaluate ice thickness and bedrock geometry: preliminary results from pilot tests performed in the ortles-cevedale group (Italian alps). Ann. Geophys. 60. https://doi.org/10.4401/ag-7122.
van der Veen, C.J., 1998. Fracture mechanics approach to penetration of surface crevasses on glaciers. Cold Reg. Sci. Technol. 27, 31–47. https://doi.org/10.1016/S0165-232X(97)00022-0.
Vornberger, P.L., Whillans, I.M., 1990. Crevasse deformation and examples from Ice Stream B, Antarctica. J. Glaciol. 36, 3–10.
Williams, R.M., Ray, L.E., Lever, J.H., 2012. Autonomous robotic ground penetrating radar surveys of ice sheets: using machine learning to identify hidden crevasses. In: IST 2012 - 2012 IEEE Int. Conf. Imaging Syst. Tech. Proc. pp. 7–12. https://doi.org/10.1109/IST.2012.6295593.
Williams, R.M., Ray, L.E., Lever, J.H., Burzynski, A.M., 2014. Crevasse detection in ice sheets using ground penetrating radar and machine learning. IEEE J. Sel. Topic. Appl. Earth Obs. Remote Sens. 7, 4836–4848. https://doi.org/10.1109/JSTARS.2014.2332872.
Wright, A., Siegert, M., 2012. A fourth inventory of Antarctic subglacial lakes. Antarct. Sci. 24, 659–664. https://doi.org/10.1017/S095410201200048X.
Xu, T., Yang, W., Liu, Y., Zhou, C., Wang, Z., 2011. Crevasse detection in Antarctica using ASTER images. Image Anal. Recognit. 370–379.
Zamora, Rodrigo, Casassa, G., Rivera, A., Ordenes, F., Neira, G., Araya, L., Mella, R., Bunster, C., 2007. Crevasse detection in glaciers of southern Chile and Antarctica by means of ground penetrating radar. IAHS Proc. 318, 153–162.